

Optical conductivity from local anharmonic phonons

Hideki Matsumoto*

*Department of Physics, Graduate School of Science, Tohoku University, Sendai 980-8578 Japan
Institute for Materials Research, Tohoku University, Sendai, 980-8577 Japan and
CREST(JST), 4-1-8 Honcho, Kawaguchi, Saitama 332-0012, Japan*

Tatsuya Mori, Kei Iwamoto, Shohei Goshima, Syunsuke Kushibiki, and Naoki Toyota[†]

*Department of Physics, Graduate School of Science, Tohoku University, Sendai 980-8578 Japan
(Dated: February 12, 2009, revised May 19, 2009)*

Recently there has been paid much attention to phenomena caused by local anharmonic vibrations of the guest ions encapsulated in polyhedral cages of materials such as pyrochlore oxides, filled skutterdites and clathrates. We theoretically investigate the optical conductivity solely due to these so-called rattling phonons in a one-dimensional anharmonic potential model. The dipole interaction of the guest ions with electric fields induces excitations expressed as transitions among vibrational states with non-equally spaced energies, resulting in a natural line broadening and a shift of the peak frequency as anharmonic effects. In the case of a single well potential, a softening of the peak frequency and an asymmetric narrowing of the line width with decreasing temperature are understood as a shift of the spectral weight to lower level transitions. On the other hand, the case of a double minima potential leads to a multi-splitting of a spectral peak in the conductivity spectrum with decreasing temperature.

PACS numbers: 63.20.Ry, 63.20.Pw, 78.20.Bh

I. INTRODUCTION

Anharmonicity in lattice vibrations has been one of the old problems in condensed-matter physics^{1,2}. Anharmonic effects in acoustic phonons were treated by perturbation theory^{2,3}, while those in local vibrations were investigated in impurities or disordered systems^{4,5,6}. It was pointed out that the effects of the anharmonicity in local vibrations appear in the characteristic temperature dependence of the vibrational frequency and of the line width⁷. Since an isolated irregular atom receives an anharmonic potential from the regular lattice, analysis have been made mostly on the anharmonic oscillation receiving effects of surrounding oscillation of the regular lattice.

Recently a revised interest on anharmonic phonons has arisen in relation to a material series of pyrochlore oxides^{8,9}, filled skutterdites^{10,11,12} and clathrates^{13,14,15,16,17}. Those materials, which are usually electrical conductors like metals, semimetals or heavily-doped semiconductors, have a common feature that some numbers of atoms form a three-dimensional network of polyhedral cages, in each of which a guest ions is accommodated. When the cages are oversized, the guest ion vibrates with a large amplitude in an anharmonic potential. Such vibrations are named as *the rattling phonons*. To note, depending on kinds of guest ions, on-centering or off-centering vibrations occur even in the same cage structure.

There have been reported various anomalous phenomena in the above materials, some of which have been discussed in relation to those rattling phonons¹⁹. In applying some clathrate compounds to thermoelectric material devices, for example, the rattling phonons, in particu-

lar off-centered, are expected to suppress strongly the thermal conductivity by effectively scattering Debye-like acoustic phonons propagating through the cage network and carrying heat entropy^{15,16,17,20}. An alternative example is found in the superconductivity in a β -pyrochlore oxide KOs_2O_6 . It was suggested that rattling vibrations of the K^+ in the OsO_6 octahedral cage were responsible for the strong-coupling superconductivity and also for an electron-mass enhancement^{22,23}. It may be fair, however, to state that these interesting issues as for the question how rattling phonons interact with cage acoustic phonons and/or charge carriers are far from being well understood¹⁹.

So far lattice vibrational modes including rattling phonons in the above cage materials have been studied rather extensively with use of spectroscopic measurements such as inelastic neutron and Raman scatterings¹⁹. Some low-lying rattling modes are clarified to exhibit softening with decreasing temperatures. The softening phenomenon has been well recognized as one of the anharmonic effects from rattling phonons, which was discussed with a quasi-harmonic approximation²⁷. Beside these spectroscopies, an infrared-active optical measurements, particularly in the Terahertz range, would be, in principle, a powerful tool to clarify the charge dynamics in low-lying optical phonons near $q \sim 0$ with available optical conductivity spectra.

Recently, time-domain terahertz spectroscopy²⁸ has been successfully applied for the first time to observe the rattling phonons around 1THz in a type-I clathrate $\text{Ba}_8\text{Ga}_{16}\text{Ge}_{30}$ (BGG)²⁹. In this paper, we investigate systematically the optical conductivity spectra from the rattling phonons in an on-centered and off-centered potential, and apply the obtained theoretical classifica-

tion of the spectra to analyse the experimental result of BGG. The detail of the experiment will be presented elsewhere²⁹. We express the optical conductivity by level transitions among states in an anharmonic potential³⁰. The present analysis shows that the most important effect of an anharmonic potential is the non-equal energy spacing of level transitions, resulting in an intrinsic and asymmetric spread of the excitation spectral, in contrast to the harmonic case of the equal energy spacing simply resulting in the Lorentzian spectral shape. Also there arise variety of level schemes for low-lying states depending on an on-centered or off-centered potential. Those features induce the natural broadening of the line width at higher temperature, softening of the peak frequency³¹ and multi-peak structures at low temperature in optical conductivity.

In the present paper, a one-dimensional model is used for simplicity. Essential effects from the anharmonicity are included. In the next section, the model and the expression of the optical conductivity are presented. In Sect.3 some of numerical results are presented. Comparison with the recent experiment²⁹ is discussed. Sect.4 is devoted to the conclusion.

II. FORMULATION

As a model to describe the motion of a guest ion in the cage, we take the following one-dimensional anharmonic potential model, for simplicity,

$$H = \frac{p^2}{2M} + \frac{1}{2}kx^2 + \frac{1}{4}\lambda x^4, \quad (2.1)$$

where M , p and x are the mass, momentum and spatial coordinate of the guest ion, respectively. We neglect effects of acoustic phonons and electrons.

The optical conductivity from the guest ion is obtained by considering the polarization induced by an applied oscillatory electric field $E(t)$,

$$H_I = -qE(t)x, \quad (2.2)$$

where q is the charge of the guest ion. By use of the linear response theory, the polarization $P(t)(= \langle qx(t) \rangle)$ is obtained as

$$P(t) = \frac{i}{\hbar} \int dt' q^2 \langle Rx(t)x(t') \rangle E(t'), \quad (2.3)$$

where $\langle \dots \rangle$ indicates the thermal average and "R" means the retarded function. By taking the Fourier transform, the polarizability $\alpha(\omega)$ defined by

$$P(\omega) = \alpha(\omega)E(\omega) \quad (2.4)$$

is obtained as

$$\alpha(\omega) = -\frac{q^2 N}{\hbar} G_{xx}(\omega), \quad (2.5)$$

where the density of the guest ion N is taken into account and $G_{xx}(\omega)$ is defined by

$$\langle Rx(t)x(t') \rangle = \frac{i}{2\pi} \int d\omega e^{-i\omega(t-t')} G_{xx}(\omega). \quad (2.6)$$

Let us denote eigenstates and eigenvalues of the Hamiltonian H by $|n\rangle$ and E_n , respectively,

$$H|n\rangle = E_n|n\rangle. \quad (2.7)$$

Then $G_{xx}(\omega)$ is expressed as

$$G_{xx}(\omega) = \sum_{nm} |\langle n|x|m \rangle|^2 \frac{(e^{-\beta E_m} - e^{-\beta E_n})/Z}{\omega + i\Gamma_0/2 - (E_n - E_m)/\hbar} \quad (2.8)$$

with $\beta = 1/k_B T$ and $Z = \sum_n e^{-\beta E_n}$. Here we have introduced a phenomenological parameter of the decay width Γ_0 . Since the optical conductivity and the polarizability are related to each other as

$$\sigma(\omega) = -i\omega\alpha(\omega), \quad (2.9)$$

we have the complex optical conductivity as

$$\begin{aligned} \sigma(\omega)/\sigma_0 &= i\omega \sum_{\omega_{nm} > 0} |\langle n|(x/x_0)|m \rangle|^2 \frac{e^{-\beta E_m} - e^{-\beta E_n}}{Z} \\ &\times \left(\frac{1}{\omega - \omega_{nm} + i\Gamma_0/2} - \frac{1}{\omega + \omega_{nm} + i\Gamma_0/2} \right) \end{aligned} \quad (2.10)$$

with

$$\omega_{nm} = (E_n - E_m)/\hbar. \quad (2.11)$$

Hereafter, we use the notation E_{nm} , ω_{nm} and ν_{nm} , respectively, as the energy, angular frequency and frequency for the transition from the m -state to the n -state. The normalization for the conductivity σ_0 is given by

$$\sigma_0 = q^2 N x_0^2 / \hbar. \quad (2.12)$$

with a length scale x_0 determined shortly. In the following analysis, we choose a suitable energy scale $\hbar\omega_0$, which can be, for example, the energy corresponding to 1THz or a harmonic frequency evaluated from the quadratic term in the potential, or an observed phonon energy. The scaled parameters are defined as

$$\bar{k} = \frac{k}{M\omega_0^2}, \quad \bar{\lambda} = \frac{\hbar\lambda}{M^2\omega_0^3}. \quad (2.13)$$

and the length scale x_0 is given as

$$x_0 = \sqrt{\frac{\hbar}{M\omega_0}}. \quad (2.14)$$

In the next section, we will calculate $\sigma(\omega)$ for cases of $k > 0$, $k = 0$ and $k < 0$, and discuss characteristic features of the optical conductivity from the rattling phonon.

III. NUMERICAL ANALYSIS

A. The case of $k > 0$

We can choose $\bar{k} = 1$ without loss of generality. In this case, ω_0 is given by $\omega_0 = \sqrt{k/M}$, the harmonic frequency. Let us estimate the magnitude of $\bar{\lambda}$. In the band structure calculation for $\text{Ba}_8\text{Ga}_{16}\text{Ge}_{30}$ ³², the coefficients k and λ were evaluated as $ka_B^2/2 = 2.813\text{mRy}$ and $\lambda a_B^4/4 = 1.602\text{mRy}$, where a_B is the Bohr radius. Then using the mass of the Ba-atom 137.35 a.u., we have the harmonic frequency $\nu_0 = 0.6975\text{THz}$ and $\bar{\lambda} = 4.292 \times 10^{-2}$. The actually observed phonon frequency lowest lying in $\text{Ba}_8\text{Ga}_{16}\text{Ge}_{30}$ is about 1THz and the parameters k may vary about twice or so. Taking into account the above estimation and Eq. (2.13), we take the value of $\bar{\lambda}$ in the range of $\bar{\lambda} = 0.0 - 0.05$.

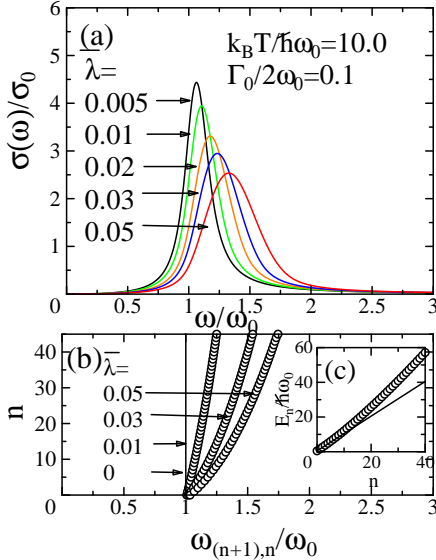


FIG. 1: (Color online) (a) Optical conductivity for various $\bar{\lambda}$ with $\bar{k} = 1$ at $k_B T/\hbar\omega_0 = 10.0$, (b) excitation energy ω_{10} and (c) energy eigenvalues for $\bar{\lambda} = 0.05$.

In Fig. 1 (a) we plot the optical conductivity for various $\bar{\lambda}$ at $k_B T/\hbar\omega_0 = 10.0$. Hereafter, we introduce a constant decay width $\Gamma_0/2\omega_0 = 0.1$ by hand, in order to smooth the frequency dependence of the optical conductivity. How each level transition has a decay width depends on interactions with electrons or acoustic phonons. Details of such effects are not considered in this paper. Also in the following, $\sigma(\omega)$ denotes the real part of the complex conductivity. At $\bar{\lambda} = 0$, the phonon mode has the single angular frequency $\omega = \omega_0$, and the line width is the decay width Γ_0 . As $\bar{\lambda}$ increases, both of the peak position and the line width increase. That is, the line width at higher temperature is determined by the anharmonic parameter $\bar{\lambda}$. In Fig. 1 (b), we plot the excitation energy $\omega_{(n+1),n} = (E_{n+1} - E_n)/\hbar$. This is obtained by calculating the energy eigenvalues numerically. One

example of the behavior of energy eigenvalues is shown in Fig. 1(c) for $\bar{\lambda} = 0.05$. The label "n" is identical with the boson number in the harmonic case of $\bar{\lambda} = 0$. The energy eigenvalues deviate from the linear behavior as $E_n \approx e_0 + e_1 n + e_2 n^2$ but a perturbation calculation is not applicable, since $\bar{\lambda} n^2$ becomes an order of one for $n \sim 10$. The calculation shows that the transition probability arises mostly from $\langle n+1|x|n \rangle$. As is seen in Fig. 1(b), the excitation energies increase as eigenvalues (i.e. n) increase due to the anharmonicity; the larger the $\bar{\lambda}$, the more spreading excitation energies become. The non-equal energy spacing of the phononic level transitions leads to the intrinsic spread of the line width in the optical conductivity, as is seen in Fig. 1(a). It should be noted that excitations with larger n (~ 30) contribute at $k_B T/\hbar\omega_0 = 10$.

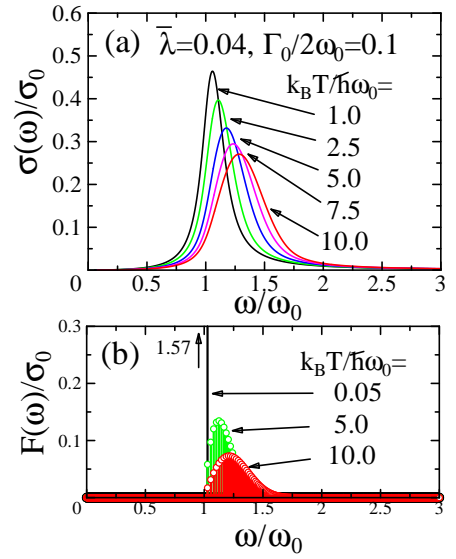


FIG. 2: (Color on line) (a) Temperature dependence of the optical conductivity for $\bar{\lambda} = 0.04$ and $\bar{k} = 1$. (b) The corresponding spectral weight at $k_B T/\hbar\omega_0 = 0.05, 5.0$ and 10.0 .

In Fig. 2(a), we plot the temperature dependence of the optical conductivity. The optical conductivity shows the softening of the peak position and the narrowing of the line width with decreasing temperature. At low temperature, only the first level transition contributes. As temperature increases, the transition involves higher energy levels, resulting in a shift of the effective peak position. Also the line width increases, since more level transitions contribute. In order to see the line-distribution without the smoothening by the width Γ_0 , we plot, in Fig. 2(b), the spectral weight in the optical conductivity given by

$$F(\omega)/\sigma_0 = \pi \sum_{\omega_{nm}=\omega} |\langle n|\xi|m \rangle|^2 \frac{e^{-\beta E_m} - e^{-\beta E_n}}{Z} \quad (3.1)$$

for $k_B T/\hbar\omega_0 = 0.05, 5.0$ and 10.0 . Sharp lines arising from the non-equal spacing of the level transitions dis-

tribute rather densely in the present parameter values. Because of the Boltzmann factor and a factor n from $|\langle n|\xi|n \pm 1\rangle|^2$, the maximum position of the weight increases with temperature and decreases exponentially as the energy $\hbar\omega$ increases. At $T = 0\text{K}$, the main contribution arises from the transition between the ground state and the first excited state. The softening of the peak frequency and the sharpening of the line width with decreasing temperature are direct consequences derived solely from an inequivalence of the level spacing that is essential in the anharmonicity. Therefore measurements on the temperature dependence of the optical conductivity can provide a direct evidence for the anharmonicity.

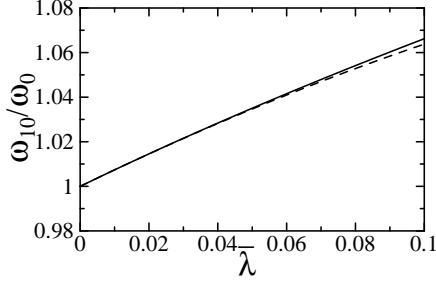


FIG. 3: $\bar{\lambda}$ -dependence of ω_{10} for $\bar{k} = 1$

In Fig. 3 the transition energy for the $0 \rightarrow 1$ transition is shown, which gives the peak frequency at $T = 0\text{K}$. In the present parameter region, the curve is fitted by

$$\omega_{10}/\omega_0 = 1 + 0.7414\bar{\lambda} - 0.7998\bar{\lambda}^2, \quad (3.2)$$

which deviates above $\bar{\lambda} \sim 0.05$ from the result of the perturbation, $\omega_{10} = 1 + (3/4)\bar{\lambda} - (9/8)\bar{\lambda}^2$ (dashed line).

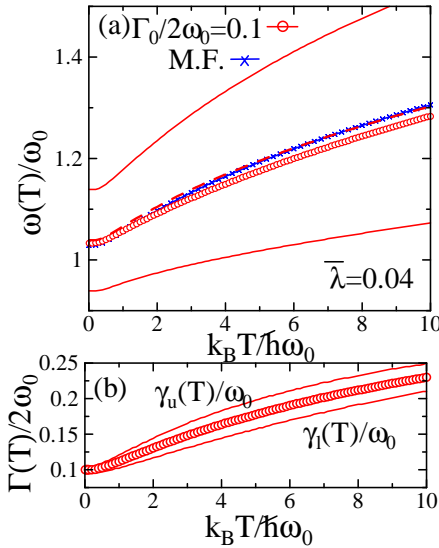


FIG. 4: (Color online) Temperature dependence of (a) the peak position and (b) line width for $\bar{\lambda} = 0.04$ and $\bar{k} = 1$

In Fig. 4 (a) we plot the temperature dependence of the peak frequency for $\Gamma_0/2\omega_0 = 0.1$ (red circles) and,

by red solid lines, upper and lower energies which give half values of the peak intensities. The red dashed line is for their averaged energy (say, mid-frequency). The blue diagonal-crosses indicate the result obtained from the following equation in the mean field theory²⁷ (The factor 3 is corrected.),

$$\frac{\omega^2}{\omega_0^2} = 1 + 3\bar{\lambda} \frac{\omega_0}{\omega} \left(\frac{1}{\exp\left(\frac{\hbar\omega_0}{k_B T} \frac{\omega}{\omega_0}\right) - 1} + \frac{1}{2} \right). \quad (3.3)$$

We see that the averaged value (red dashed line) well agree with the mean field results (blue diagonal-crosses). However, our result of the peak structure is asymmetric, reflecting the spectral weight, Eq. (3.1). We express the line width at temperature T as

$$\Gamma(T) = \gamma_u(T) + \gamma_l(T) \quad (3.4)$$

with $\gamma_u(T)$ ($\gamma_l(T)$) being the upper (lower) half width from the peak frequency, which is shown in Fig. 4 (b). The saturation of the line width is due to the decay width Γ_0 , which may originate from a phonon-electron interaction and a rattling phonon-acoustic phonon interaction neglected in this paper. However, at higher temperature, $\Gamma(T)$ increases fairly larger than Γ_0 . Also the broadening in upper and lower frequency is asymmetric. The line broadening due to the anharmonicity leads to a non-Lorentzian spectral shape.

From the analysis of this subsection, we see that anharmonicity of the rattling phonon leads to softening of the phonon frequency and sharpening and asymmetric change of the line width with decreasing temperature.

B. $k = 0$

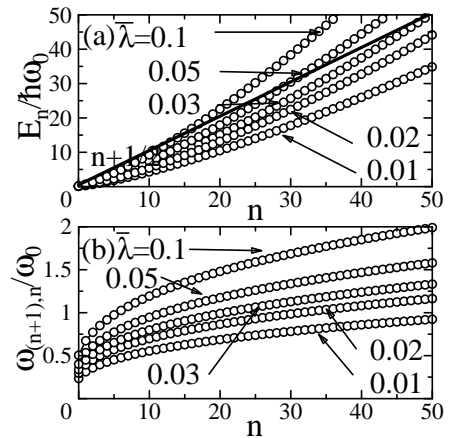


FIG. 5: (a) Energy eigenvalues and (b) excitation energy for $\bar{k} = 0$

When $k = 0$ (or $|k| \ll \lambda a_B^2$), the peak position and the line width are solely determined by λ . We choose

$\hbar\omega_0$ as a characteristic energy of the system, for example, $\omega_0/2\pi=1\text{THz}$. In Figs. 5 (a) and (b), the energy eigenvalues and the excitation energy $\omega_{(n+1),n} = (E_{n+1} - E_n)/\hbar$ are plotted. The lower excitation energies are softened and, just as well as in the case of $k > 0$, the effectively contributing n decreases with decreasing temperatures, resulting in the characteristic behavior, softening and sharpening, of the optical conductivity as is shown in Figs. 6 and 7. Note that the lowest excitation energy is softened up to about a half of the characteristic energy because of the shallow shape of the potential bottom.

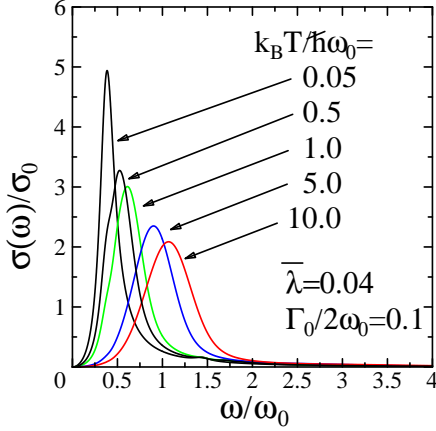


FIG. 6: (Color online) Temperature dependence of the optical conductivity for $\bar{\lambda} = 0.04$ and $\bar{k} = 0$.

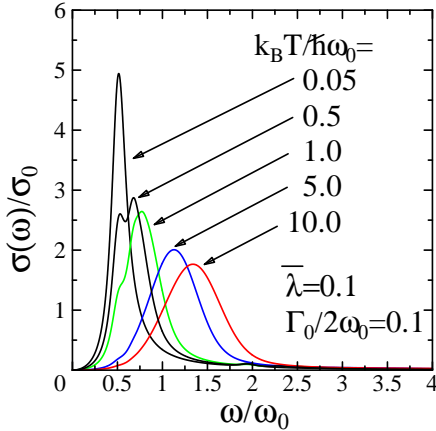


FIG. 7: (Color online) Temperature dependence of the optical conductivity for $\bar{\lambda} = 0.1$ and $\bar{k} = 0$.

In the case of $\bar{\lambda} = 0.04$ (Fig. 6), the difference of the neighboring excitation energies is less than Γ_0 , so that the optical conductivity shows a smooth softening, though the shift is enlarged and some shoulder is seen at low temperature ($k_B T / \hbar\omega_0 = 0.5$). Such a shoulder structure is smoothed for a smaller $\bar{\lambda}$. When $\bar{\lambda}$ becomes large, the difference of the lower excitation energies exceeds Γ_0 , and as in Fig. 7 the optical conductivity shows

a double peak structure as temperature decreased. The upper peak is reduced as temperature is further lowered. The broadening of the line width at higher temperature is enhanced as $\bar{\lambda}$ increases.

C. The case of $k < 0$

For negative k , the anharmonic potential has double minima. We investigate the temperature dependence of the optical conductivity for $\bar{\lambda} = 0.04$ by changing \bar{k} . Depending on the depth of the double minima, various patterns of temperature-dependent optical conductivity are obtained. We choose $\hbar\omega_0$ as a characteristic energy of the system, for example, $\omega_0/2\pi=1\text{THz}$.

In Fig. 8, we show the temperature dependence of the optical conductivity for various \bar{k} . The softening of the peak position is seen in Figs. 8(a)-(c), but in Figs. 8(d)-(f) the softening of the peak frequency is followed by the hardening, with decreasing temperature.

Low temperature behaviors have various variety, especially there appear structures with double or triple peaks, though it depends on the magnitude of the width Γ_0 . This can be understood from the low energy level transition in the double well potential. In Fig. 9(a), one example of the potential with $k < 0$ is illustrated together with the eigenenergy levels. Low energy levels are much modified by the depth of the potential well. In Fig. 9(b) the \bar{k} -dependence of E_n for low energy levels are plotted. Dotted lines are the potential double minima with the value $V(\pm\sqrt{-k/\bar{\lambda}})/\hbar\omega_0 = -\bar{k}^2/4\bar{\lambda}$ and the local maximum $V(0) = 0$, respectively. When $-\bar{k}$ increases, the levels (E_0, E_1) , (E_2, E_3) , \dots , successively degenerate forming low-lying tunneling modes. In Fig. 9(c) the transition energies ω_{nm} are plotted among low-lying eigenstates. The dotted line is for the depth of the potential well. Transition energies ω_{10} and ω_{32} show successively softening as $-\bar{k}$ increases, while the neighboring excitations ω_{21}, ω_{43} increase and become larger than excitation energies among higher levels ($\omega_{11,10}$ in Fig. 9(c)). The upturn of the excitation energies of ω_{21} is correlated with the depth of the potential well. In the following we discuss more details of low temperature behaviors in Fig. 8.

Figs. 8(a) and (b) are for shallow double wells. Transition energy of $\hbar\omega_{10}$ is softened and it becomes smaller than $\hbar\omega_{21}$ due to the effect of the double well. Further, $(\omega_{21} - \omega_{10})$ is larger than Γ_0 , so that there appears two peaks at low temperature and the higher peak of ω_{21} diminishes as $T \rightarrow 0\text{K}$. The peak around $\omega/\omega_0 = 1$ which remains even at $T = 0\text{K}$ corresponds to the transition $\hbar\omega_{30}$.

Fig. 8(c) is for $\bar{k} = -0.3$. The states 0 and 1 become very close but still have finite difference. We can identify lower peak as ω_{10}, ω_{21} and ω_{30} . The peak for ω_{21} is reduced with decreasing temperature (See also Fig. 9(c)).

Fig. 8(d) is for $\bar{k} = -0.4$. The states 0 and 1 are almost degenerate, and this soft mode does not appear

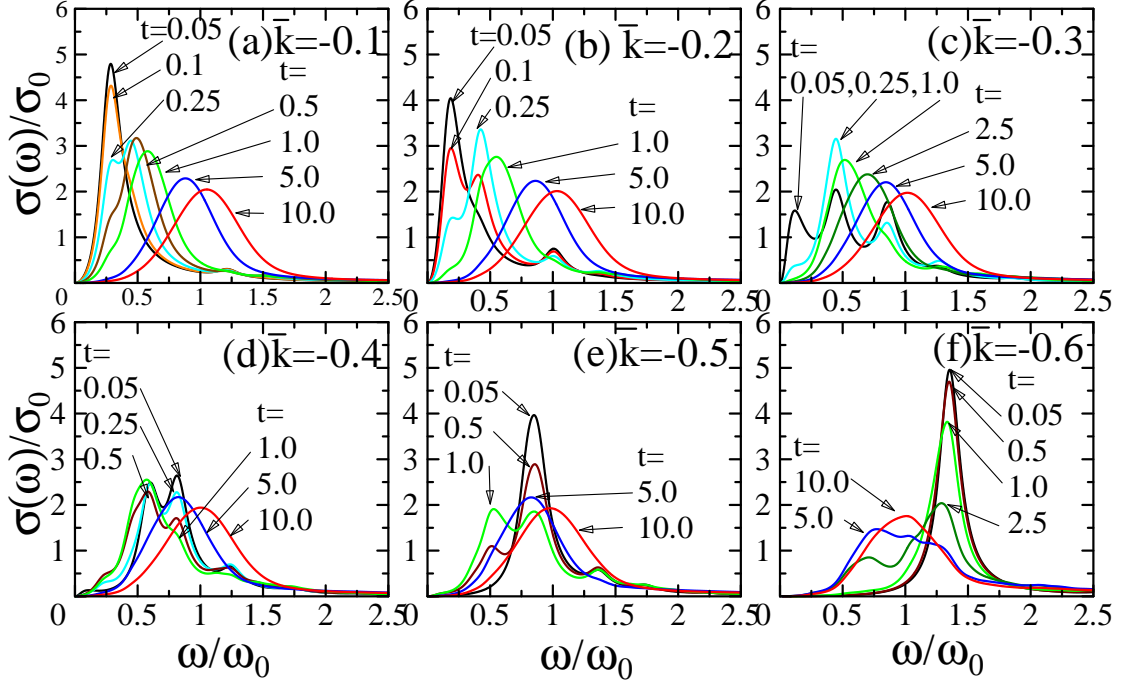


FIG. 8: (Color online, Wide figure) Temperature dependence of the optical conductivity for various $\bar{k} < 0$. Parameters are $\bar{\lambda} = 0.04$, $\Gamma_0/2\omega_0 = 0.1$. t is the reduced temperature $t = k_B T / \hbar \omega_0$.

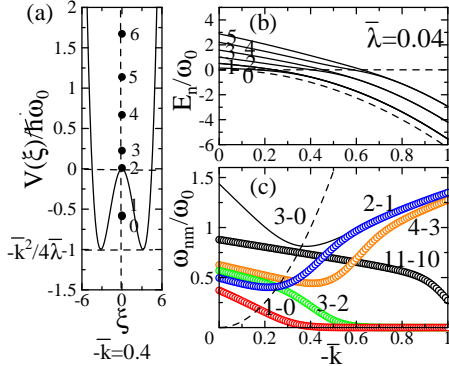


FIG. 9: (Color online) (a) Schematics of the double-minima potential and energy levels for $\bar{k} = -0.4$, and k -dependence of (b) E_n and (c) ω_{nm} for low energy levels. $\bar{\lambda}$ is chosen as 0.04.

in the optical conductivity because of the factor ω in Eq. (2.10). The state 2 is inside the double well and the state 3 is above the maximum at $x = 0$. Then ω_{21} is larger than ω_{32} . We can identify the peaks in Fig. 8(d) as ω_{32} , ω_{12} and ω_{03} from the low energy side. Note that the intensity of the peak ω_{32} increases and decreases as temperature decreases.

In Fig. 8(e), \bar{k} is further reduced as $\bar{k} = -0.5$. The state 2 and 3 start to degenerate and ω_{32} becomes lower than ω_{21} . We can identify the peaks in Fig. 8(e) from the low energy side as ω_{43} and $(\omega_{12}, \omega_{03})$.

In Fig. 8(f), the state 2 and 3 are completely degenerate

and ω_{21} is the main transition at low temperature. Since this energy is much larger than energies for higher level transition, the peak position first decrease at higher temperature and then increase at low temperature.

When \bar{k} is further reduced and the double minima become deep enough, the hardening of the peak frequency is obtained rather than softening as was discussed in ref.³⁰.

In this way, we have various patterns depending on the strength of the double well

D. Comparison with the experiment

We have performed the time-domain THz spectroscopy and obtained the optical conductivity²⁹ in a type-I clathrate $\text{Ba}_8\text{Ga}_{16}\text{Ge}_{30}$ ^{14,15,16,32}. The details of the experimental method and analysis will be presented in a separated paper²⁹. The obtained temperature-dependence of the phonon spectral for the lowest mode ($\sim 1.2\text{THz}$) is shown by colored symbols in Fig. 10. No multi-peak structure is observed. Then from the patterns presented in this paper, we conclude $k > 0$ and we take $\bar{k} = 1$.

We adjust ω_0 , $\bar{\lambda}$, Γ_0 and σ_0 to fit overall behaviors and specially the higher frequency region ($1.25 \sim 1.40\text{THz}$) of the spectral line. We choose $\omega_0/2\pi = 1.143\text{THz}$, $\bar{\lambda} = 9.66 \times 10^{-3}$, $\Gamma_0/2\pi = 0.067\text{THz}$, and $\sigma_0 = 6.82\Omega^{-1}\text{cm}^{-1}$. Theoretical results are presented by solid lines in Fig. 10. The agreement between the experimental and theoretical results in temperature-dependence is very good.

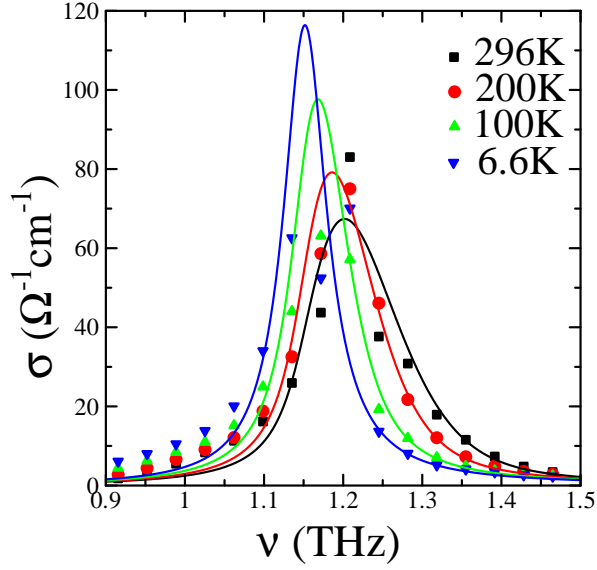


FIG. 10: (Color online) Comparison of the optical conductivity for $\text{Ba}_8\text{Ga}_{16}\text{Ge}_{30}$

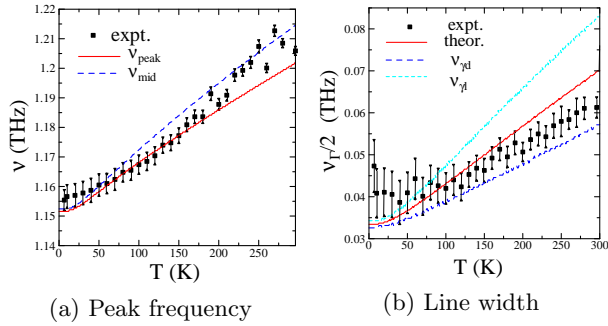


FIG. 11: (Color online) Temperature-dependence of the peak frequency and the line width

The temperature dependence of the peak frequency and the line width are estimated from the experimental data by the Lorentzian fit and are plotted by the solid rectangles in Fig. 11(a) and (b), respectively. Theoretical results are plotted by solid and dashed lines. In Fig. 11(a), the red solid line is for the peak frequency ν_{peak} and the green dashed line is for the mid-frequency ν_{mid} . In Fig. 11(b), the red solid, blue dashed and light blue short-dashed lines are frequencies $\nu_{\Gamma/2}$, ν_{γ_u} and ν_{γ_l} corresponding to the half width, the lower and upper half width, respectively. The experimental peak frequency situates between the theoretical peak and mid-frequency. Also the half-width is between the theoretical half-width and lower half-width. Since the Lorentzian fit is apt to

lead a higher peak frequency and a narrower line width in an asymmetric line shape, the agreement between the experimental and theoretical results is reasonably good. The present comparison shows that the temperature-dependence of the rattling phonon in $\text{Ba}_8\text{Ga}_{16}\text{Ge}_{30}$ is well described by the anharmonicity of the potential without considering details of effects from other interactions.

It has been reported that a type-I clathrate $\text{Ba}_8\text{Ga}_{16}\text{Sn}_{30}$ has an off-centered potential of the guest ion¹⁷. It is an interesting problem to see if the optical conductivity of this material shows a behavior with $k < 0$ discussed in this paper³³.

IV. CONCLUSION

In this paper we have investigated theoretically the temperature dependence of the optical conductivity from the rattling phonon. The guest ion feels an anharmonic potential from the cage, and the anharmonic effect appears characteristically in the temperature dependence, that is, the softening of the peak frequency and sharpening of the line width with decreasing temperature.

In the case of the positive quadratic term, one can expect the quadratic coefficient is roughly determined from the saturated peak frequency at low temperature and the quartic term is determined from the line width and shift of the peak frequency.

In the case of the negative quadratic term, various patterns of the optical conductivity are expected depending on the strength of the double minima in the potential. Multi-peak structures appear at low temperature and increase and decrease of the peak frequency with temperature are obtained.

We have shown that measurements on the temperature dependence of the optical conductivity can provide a direct evidence for the anharmonicity.

Acknowledgements

We thank Drs. M. A. Avila, J. P. Carbotte, M. Dressel, H. Hasegawa, M. Lang, H. Matsui, T. Nakayama, N. Ogita, K. Suekuni, T. Takabatake, Y. Takasu, K. Tanigaki, M. Udagawa, K. Ueda, W. Weber, A. Yamakage, A. Yoshihara, M. Yoshizawa and T. Koyama for valuable discussions. Two of us (T. M., K. I.) are supported financially by the Global COE program “Materials Integrations”, Tohoku University. This work has been supported by Grants-in-Aid for Scientific Research (A)(15201019) and the priority area “Nanospace” from MEXT, Japan.

* Electronic address: matumoto@ldp.phys.tohoku.ac.jp

† Electronic address: toyota-n@ldp.phys.tohoku.ac.jp

¹ M. Born and K. Huang, *Dynamical theory of crystal lattices*, (Oxford at the Clarendon Press, London, 1968).

- ² O. Madelung, *Introduction to solid-state theory*, (Springer-Verlag, Berlin Heidelberg New York, 1978).
- ³ P. Choquard, *The anharmonic crystal*, (W. A. Benjamin, Inc., New York, Amsterdam, 1967).
- ⁴ R. W. H. Stevenson, *Phonons in perfect lattices and in lattices with point imperfections*, (Oliver & Boyd, Edinburgh and London, 1966)
- ⁵ B. C. Newman, Adv. Phys. **18**, 545 (1969).
- ⁶ A. S. Barker Jr. and A. J. Sievers, Rev. Mod. Phys. **47**, Suppl., s1 (1975).
- ⁷ R. J. Elliot, W. Hayes, G. D. Jones, H. F. Macdonald and C. T. Sennett, Proc. R. Soc. London **289A**, 1 (1965).
- ⁸ M. A. Subramanian, G. Aravamudan and G. V. S. Rao, Prog. Solid State Chem. **15**, 55 (1983).
- ⁹ M. Hanawa, Y. Muraoka, T. Tayama, T. Sakakibara, J. Yamaura and Z. Hiroi, Phys. Rev. Lett. **87**, 187001 (2001).
- ¹⁰ W. Jeitschko and D. J. Braun, Acta Crystallogr., Sect. B: Struct. Crystallogr. Cryst. Chem. **33**, 3401 (1977).
- ¹¹ D. J. Braun and W. Jeitschko, J. Less-Common Met., **72**, 147 (1980).
- ¹² B. C. Sales, D. Mandrus, B. C. Chakoumakos, V. Keppens and J. R. Thompson, Phys. Rev. B **56**, 15081 (1997).
- ¹³ G. S. Nolas, J. L. Cohn, G. A. Slack and S. B. Schujman, Appl. Phys. Lett. **73**, 178 (1998).
- ¹⁴ B. C. Sales, B. C. Chakoumakos, R. Jin, J. R. Thompson and D. Mandrus, Phys. Rev. B **63**, 245113 (2001).
- ¹⁵ A. Bentien, M. Christensen, J. D. Bryan, A. Sanchez, S. Paschen, F. Steglich, G. D. Stucky and B. B. Iversen, Phys. Rev. B **69**, 045107 (2004).
- ¹⁶ M. A. Avila, K. Suekuni, K. Umeo, H. Fukuoka, S. Yamanaka and T. Takabatake, Phys. Rev. B **74**, 125109 (2006).
- ¹⁷ M. Avila, K. Suekuni, K. Umeno, H. Fukuoka, S. Yamanaka and Y. Takabatake, Appl. Phys. Lett. **92**, 041901 (2008).
- ¹⁸ S. Yonezawa, Y. Muraoka, Y. Matsushita and Z. Hiroi, J. Phys. Condens. Matter **16**, L3 (2004).
- ¹⁹ For recent reviews, see the special issue, J. Phys. Soc. Japan, 77 Supplement A (2008)
- ²⁰ T. Nakayama and E. Kanashita, Europhysics Letters **84**, 66001 (2008).
- ²¹ Z. Hiroi, S. Yonezawa, J. Yamaura, T. Muramatsu and Y. Muraoka, J. Phys. Soc. Jpn. **74**, 1682 (2005).
- ²² M. Bruhwiler, S.M. Kazakov, J. Karpinski and B. Batlogg, Phys. Rev. B **73**, 094518 (2006).
- ²³ Z. Hiroi, S. Yonezawa, Y. Nagao and J. Yamaura, Phys. Rev. B **76**, 014523 (2007).
- ²⁴ J. Yamaura, S. Yonezawa, Y. Muraoka and Z. Hiroi, J. Solid State Chem. **179**, 336 (2006).
- ²⁵ T. Goto, Y. Nemoto, K. Sakai, T. Yamaguchi, M. Akatsu, T. Yanagisawa, H. Hazama, K. Onuki, H. Sugawara and H. Sato, Phys. Rev. B **69**, 180511(R) (2004).
- ²⁶ M. Yoshida, K. Arai, R. Kaido, M. Takigawa, S. Yonezawa, Y. Muraoka, and Z. Hiroi, Phys. Rev. Lett. **98**, 197002 (2007).
- ²⁷ Thomas Dahm and Kazuo Ueda, Phys. Rev. Lett. **99**, 187003 (2007).
- ²⁸ T. Mori, E. J. Nicol, S. Shiizuka, K. Kuniyasu, T. Nojima, N. Toyota and J. P. Carbotte, Phys. Rev. B **77**, 174515 (2008).
- ²⁹ T. Mori, S. Goshima, K. Iwamoto, S. Kushibiki, H. Matsumoto, N. Toyota, K. Suekuni, A. M. Avila, T. Takabatake, T. Hasegawa and M. Udagawa, preprint, arXiv:0905.3610v1 (2008), to be published in Phys. Rev. B.
- ³⁰ Such an approach is also found in the analysis of the Raman scattering, C. M. Foster, M. Grimsditch, Z. Li and V. G. Karpov, Phys. Rev. Lett. **71**, 1258 (1993)
- ³¹ In ref.⁷, the hardening of the local mode with decreasing temperature was indicated because of the effect from the band phonon, and in ref.³⁰, a deep double minimum potential was considered, leading also the hardening of the local mode with decreasing temperature."
- ³² G. K. H. Madsen and G. Santi, Phys. Rev. B **72**, 220301(R) (2005).
- ³³ (private communication) A preliminary experiment of the optical conductivity for $\text{Ba}_8\text{Ga}_{16}\text{Sn}_{30}$ were performed, and the rattling phonon around 0.6THz has been observed. The result shows a different behavior from that of $\text{Ba}_8\text{Ga}_{16}\text{Ge}_{30}$; though the softening is also observed, the line width becomes wider in low temperature, showing some indication of a double-peak structure (T. Mori, S. Goshima, K. Iwamoto, H. Matsumoto, N. Yoyota, K. Suekuni, M. A. Avella and T. Takabatake, Reports (22pWF-3 and 22pWF-4) in the Autumn Meeting, the Physical Society of Japan, Sept. 20-23, 2008). An improvement of the signal-noise ratio in the low frequency region is in progress.